JACS
JOURNAL OF THE AMERICAN CHEMICAL SOCIETY

Communication

pubs.acs.org/JACS

Chirality Enriched (12,1) and (11,3) Single-Walled Carbon Nanotubes for Biological Imaging

Shuo Diao,[†,§] Guosong Hong,[†,§] Joshua T. Robinson,[†] Liying Jiao,[‡] Alexander L. Antaris,[†] Justin Z. Wu,[†] Charina L. Choi,[†] and Hongjie Dai*[,†]

[†]Department of Chemistry, Stanford University, Stanford, California 94305, United States

[‡]Department of Chemistry, Tsinghua University, Beijing 100084, P. R. China

Supporting Information

ABSTRACT: The intrinsic band gap photoluminescence of semiconducting single-walled carbon nanotubes (SWNTs) makes them promising biological imaging probes in the second near-infrared (NIR-II, 1.0−1.4 μm) window. Thus far, SWNTs used for biological applications have been a complex mixture of metallic and semiconducting species with random chiralities, preventing simultaneous resonant excitation of all semiconducting nanotubes and emission at a single well-defined wavelength. Here, we developed a simple gel filtration method to enrich semiconducting (12,1) and (11,3) SWNTs with identical resonance absorption at ∼808 nm and emission near ∼1200 nm. The chirality sorted SWNTs showed ∼5-fold higher photoluminescence intensity under resonant excitation of 808 nm than unsorted SWNTs on a per-mass basis. Real-time *in vivo* video imaging of whole mouse body and tumor vessels was achieved using a ∼6-fold lower injected dose of (12,1) and (11,3) SWNTs (∼3 μg per mouse or ∼0.16 mg/kg of body weight vs 1.0 mg/kg for unsorted SWNTs) than a previous heterogeneous mixture, demonstrating the first resonantly excited and chirality separated SWNTs for biological imaging.

Single-walled carbon nanotubes (SWNTs) have shown promise for biological and medical applications[1] due to their intrinsic photoluminescence,[2,3] ability to load targeting ligands and chemotherapy drugs,[4] and high efficiency for photothermal therapy.[5,6] In particular, photoluminescence in the second near-infrared window (NIR-II, 1.0−1.4 μm) provides an ideal probe for biological imaging deep inside the body, due to the low indigenous tissue autofluorescence and the much reduced photon scattering in the NIR-II region compared to in the visible (400−750 nm) and traditional NIR (NIR-I, 750−900 nm) regions.[7] However, the coexistence of metallic and semiconducting SWNTs of various diameters and chiralities in as-grown materials has limited the use of nanotubes in biological systems. Unlike regular fluorophores in the visible and NIR-I regions, as-made SWNTs contain a mixture of >20 chiralities[2,3,7−10] with various excitation peaks in the visible and NIR-I regions and emission peaks in the NIR-II region. Only a small fraction of nanotubes (<9%)[9,10] can be resonantly excited under a single excitation source, such as the 808 nm laser often used for NIR fluorescence imaging. Chirality pure SWNTs exhibiting strong emission under a well-defined resonance excitation would be much more effective NIR-II fluorophores and more desired for *in vivo* NIR-II fluorescence imaging. Diameter and chirality sorted nanotubes would also eliminate the problem of high inhomogeneity of SWNTs and enable ultralow doses of SWNTs for *in vivo* applications. Thus far, much progress has been made in separating SWNTs by diameter and chirality, including dielectrophoresis,[11] density gradient centrifugation,[12] DNA wrapping chromatography,[13] and gel filtration.[14−16] However, chirality separation of nanotubes with sufficient quantity and biocompatible functionalization has remained elusive. Moreover, the fluorescence quantum yield of SWNTs must be retained through the chirality separation and biocompatible functionalization steps in order to develop bright, homogeneous SWNT NIR-II imaging probes.

Here, we present a simple gel filtration method to selectively sort and isolate (12,1) and (11,3) chiralities that are in strong resonance with 808 nm excitation. Among various chiralities of semiconducting SWNTs, it is found that the (12,1) and (11,3) SWNTs can be coated to the highest degree by a unique combination of surfactants to give the weakest interaction with an allyl dextran-based size-exclusion gel, affording the earliest elution. The chirality sorted (12,1) and (11,3) SWNTs (CS-SWNTs) exhibit spectrally confined NIR-II emission near ∼1200 nm under 808 nm excitation and act as a single fluorophore in the NIR-II region. Furthermore, the CS-SWNTs exhibit a ∼5-fold higher NIR-II fluorescence brightness than unsorted SWNTs on the per-mass basis. Upon surfactant exchange to achieve high biocompatibility,[8] an ultralow injection dose of CS-SWNTs of 0.16 mg/kg of body weight is used to successfully perform *in vivo* imaging of the inner organs and tumor vasculatures of mice at high spatial resolution (down to <10 μm) and deep body penetration (several millimeters).

CS-SWNTs were achieved using an allyl dextran-based size-exclusion gel (Sephacryl S-200, GE Healthcare) as a medium for gel filtration.[14−16] As-made high-pressure CO conversion (HiPCO) SWNTs sample was dispersed in water with 1 wt % sodium cholate (SC) via bath sonication for 1 h. The resulting black suspension was ultracentrifuged to remove a large portion of bundled nanotubes and aggregates. The supernatant was then collected and mixed with an equal volume amount of 1 wt

Received: August 10, 2012
Published: October 3, 2012

   dx.doi.org/10.1021/ja307966u | J. Am. Chem. Soc. 2012, 134, 16971−16974

% sodium dodecyl sulfate (SDS) before adding to a 1 cm diameter column filled with 20 mL of allyl dextran-based size-exclusion gel. Metallic nanotubes were covered better by surfactant molecules than semiconducting nanotubes,[17] resulting in weaker interactions with the gel, and therefore were collected in the unbound fraction passing directly through the column. A mixture of surfactants of 0.5 wt % SC and 0.5 wt % SDS was used to further remove any metallic SWNTs, leaving purely semiconducting SWNTs of various chiralities trapped in the column.

Next, we exploited the different interaction strengths of various semiconducting SWNTs with the gel as a basis for chirality sorting.[14,18] We found that by using an eluent of 1.2 wt % aqueous SDS solution to wash the column, a narrow band containing mainly two chiralities (12,1) and (11,3) was selectively eluted (Figure 1a), while the rest of semiconducting

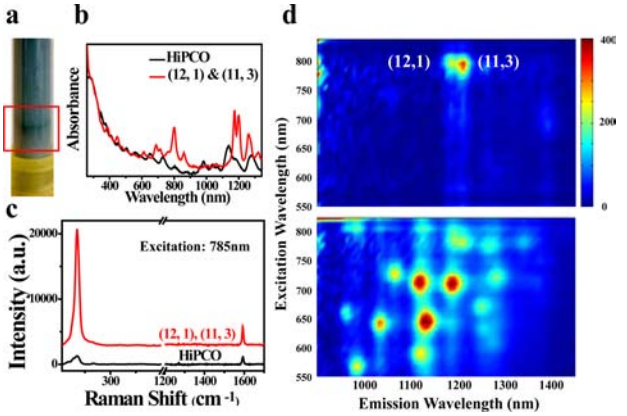

Figure 1. Chirality sorting of SWNTs. (a) Column during separation of (12,1) and (11,3) CS-SWNTs. A dark band containing (12,1) and (11,3) SWNTs can be seen in the middle of the red box drawn to highlight the band. (b) UV–vis NIR absorption and (c) Raman spectra of the CS-SWNTs and pristine HiPCO SWNTs normalized to the same mass concentration (~1 mg/L); 785 nm excitation was used for Raman spectroscopy. (d) 2D plots of PLE maps of CS-SWNTs (top) and unsorted HiPCO SWNTs (bottom). Each bright spot on the plot corresponds to semiconducting SWNTs with a certain chirality. Results here demonstrated that (12,1) and (11,3) SWNTs were highly enriched in the CS-SWNTs sample compared to the starting HiPCO SWNTs.

SWNTs remained trapped in the column. This rapid, simple gel filtration method affords (12,1) and (11,3) CS-SWNTs useful for biological imaging.

The UV–vis NIR absorption spectra of the unsorted HiPCO SWNTs and CS-SWNTs exhibited marked differences (Figure 1b). The absorption spectra confirmed that the starting sample included a variety of chiralities and a wide diameter distribution, whereas the CS-SWNTs exhibited a much narrower diameter distribution and were highly enriched with (12,1) and (11,3) SWNTs, both in close resonance with the 808 nm laser light. Spectral fitting of the UV–vis NIR absorption spectrum of CS-SWNTs revealed the purity of the two species combined as 64%.[12,14] The photoluminescence vs excitation (PLE) maps of the CS-SWNTs and unsorted sample in Figure 1d demonstrated the high degree of enrichment of (12,1) and (11,3) chiralities, evidenced by two distinct PLE spots. The spectral proximity between the two types of SWNTs enabled them to act as a single NIR-II fluorophore excited by ~808 nm and emitting at ~1200 nm. White light bright-field images of the unsorted HiPCO SWNTs and CS-SWNTs in Figure 2a showed the distinct difference in colors, suggesting successful chirality

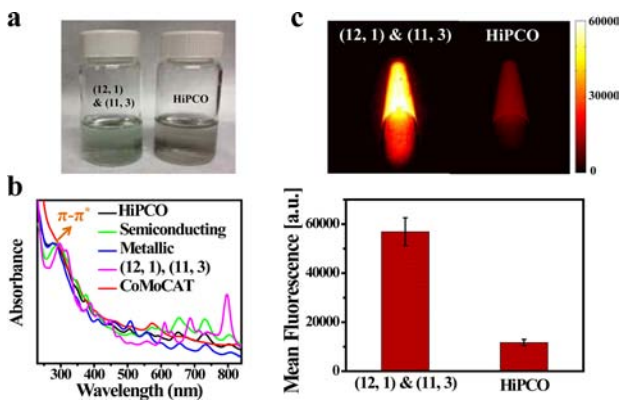

Figure 2. Optical images and NIR-II photoluminescence images of the CS-SWNTs and pristine HiPCO SWNTs. Both samples were normalized to the same mass concentration. (a) CS-SWNTs and pristine HiPCO SWNTs showing distinct colors. (b) Mass normalization for various nanotube suspensions. The π–π^* interband transition peak at ~4.5 eV (~276 nm, indicated by π–π^*) was used for mass concentration normalization for various SWNT solutions including semiconducting and metallic fractions of HiPCO SWNTs, unsorted HiPCO SWNTs, the (12,1) and (11,3) CS-SWNTs, and CoMoCAT (SouthWest NanoTechnologies) nanotubes. (c) Histogram of NIR-II photoluminescence (bottom) showed that the CS-SWNTs resulted in a significant ~5.0 fold increase in the NIR-II fluorescence intensity compared to the unsorted HiPCO mixture (see NIR-II fluorescence images on top).

sorting. Atomic force microscopy (AFM) analysis showed longer average length of CS-SWNTs than pristine SWNTs (Figure S1).

Raman spectroscopy of the starting material and CS-SWNTs was performed using a 785 nm laser excitation (Figure 1c), close to the E_{22} absorption of (12,1) and (11,3) SWNTs to afford strong resonant Raman scattering. (12,1) and (11,3) SWNTs showed strongly enhanced peaks in the radial breathing mode (RBM) region compared to a mass-normalized unsorted mixture (see below). The extremely low D band intensity in the Raman spectra suggested minimal defects on the nanotubes separated by the gel filtration process.

To evaluate the relative fluorescence brightness of CS-SWNTs compared to the unsorted starting material, we examined the NIR-II photoluminescence upon excitation of an 808 nm laser diode (Figure 2c). In order to normalize the samples to the same mass concentration, a UV–vis NIR absorption-based approach[19,20] was used (Figure 2b). The π–π^* interband transition peak at ~4.5 eV (~276 nm) was used for mass concentration normalization for various SWNT solutions (see Experimental Section in Supplementary Information). This transition was independent of surfactant coating and dielectric environment.[19,20] We found that mass-normalized CS-SWNTs exhibited a ~5.0 fold increase in NIR-II fluorescence intensity (1100–1400 nm) at 808 nm excitation compared to the unsorted mixture (Figure 2c).

To make the brightly fluorescent CS-SWNTs biocompatible for *in vivo* use, we exchanged the SC and SDS surfactants on the nanotubes to phospholipid-polyethylene glycol (PL-PEG) using a method developed by our group previously.[8] We added to the CS-SWNTs suspension 1 mg/mL of 1,2-distearoyl-*sn*-glycero-3-phosphoethanolamine–*N*-[methoxy(polyethylene

dx.doi.org/10.1021/ja307966u | J. Am. Chem. Soc. 2012, 134, 16971–16974

glycol)5000] (DSPE-mPEG(5k)), followed by a brief sonication of ~2 min to fully dissolve the polymer surfactant. The solution was then dialyzed in a 3500 molecular weight cutoff (MWCO) membrane against deionized water. After dialysis, the solution was centrifuged (16 000 g, 5 min) to remove any bundles formed during the exchange process. A small decrease in quantum yield by ~10% was observed after surfactant exchange process (Figure S2), which was likely due to mild damage induced to the SWNTs by sonication in the DSPE-mPEG surfactant.[8] Nevertheless, the relatively high fluorescence of CS-SWNTs enabled low doses of SWNTs for *in vivo* biological imaging.

We intravenously injected the DSPE-mPEG coated CS-SWNTs into nude mice for *in vivo* NIR-II imaging. Nude mice (n = 3) were injected with 200 μL of ~16 mg/L of CS-SWNTs (3 μg per mouse or 0.16 mg/kg of body weight, calculated based on the normalization method in Figure 2b and a mass extinction coefficient of 0.0465 l mg^{-1} cm^{-1} for HiPCO SWNTs)[21] into the tail vein. At a low magnification, the whole body of the mouse was included in the field of view for deep inner organ registration based on the NIR-II fluorescence of CS-SWNTs. NIR-II fluorescence images were recorded at video rate (14.5 frames/s) by detecting NIR-II fluorescence in the 1100−1400 nm range with an InGaAs camera under illumination of an 808 nm laser diode at a power density of 0.14 W/cm^2. This laser power density was well within the safe exposure limit of 0.329 W/cm^2 at 808 nm.[22] Bright-field and NIR-II photoluminescence images of the injected solution were shown in Figure 3a. As shown in the SI movie and Figure 3,

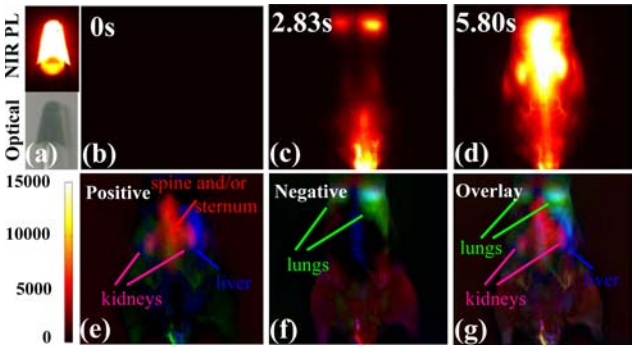

Figure 3. *In vivo* whole-animal fluorescence imaging using intravenously injected (12,1) and (11,3) CS-SWNTs. (a) Optical and photoluminescence images of a 200 μL injected CS-SWNT solution with a nanotube concentration of 0.016 mg/mL. (b) An initial NIR-II fluorescence image of a nude mouse before injection of CS-SWNTs. No signal can be discerned. (c,d) NIR-II fluorescence images shortly after injection of the CS-SWNTs. (e,g) PCA images of the positive, negative, and overlaid components. The lungs are color coded in green, the kidneys are in pink, and the liver is in blue.

bright NIR-II fluorescence in the lungs was seen immediately after intravenous injection of the CS-SWNTs (Figure 3c), corresponding to the pulmonary flow of SWNT-rich blood for oxygenation. Following the pulmonary circulation, major organs in the systemic circulation including kidneys and liver also appeared at 5.80 s post injection (p.i.) (Figure 3d). To distinguish different organs appearing sequentially during blood circulation, principal component analysis (PCA) was used to convert the temporal difference into dynamically enhanced contrast with spatial registration.[7,23] Figure 3e−g showed positive and negative PCA components, and the overlaid image derived from video rate NIR-II fluorescence images. The lungs, kidneys, and liver of the mouse were clearly distinguished by various false colors by the PCA analysis. This demonstrated for the first time that (12,1) and (11,3) chirality sorted SWNTs were used for *in vivo* imaging. Previous work to achieve organ registration based on PCA required a dose of ~1.0 mg/kg of body weight for unsorted HiPCO SWNTs.[7] With CS-SWNTs, we were able to reduce the dose by ~6-fold to obtain similar imaging results.

Not only can the chirality pure SWNTs be used for imaging inner organs *in vivo* at the whole-body magnification, as bright NIR-II fluorophores they can also be used as vascular contrast agents with microscopic resolution. We performed tumor angiography using the NIR-II fluorescence of CS-SWNTs. In a typical experiment, a 200 μL suspension of CS-SWNT at 16 mg/L (3 μg per mouse, or 0.16 mg/kg of body weight) was injected intravenously into a mouse with a subcutaneous xenograft 4T1 murine tumor located on the right shoulder (Figure 4a inset). Owing to the relatively long blood circulation

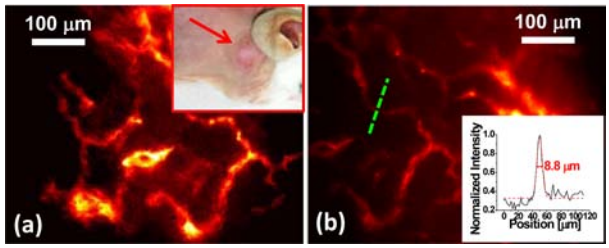

Figure 4. Xenograft tumor angiography using chirality enriched (12,1) and (11,3) SWNTs as NIR-II contrast agents. (a,b) NIR-II fluorescence images of 4T1 murine tumor vasculatures under illumination at 785 nm through a 10× microscope, focused at 2 mm underneath the surface of the tumor. The minimum resolvable vessel width is <10 μm. The inset in (a) shows the location of the inoculated 4T1 murine tumor on the right shoulder of the mouse, indicated by a red arrow, and the inset in (b) shows the cross-sectional NIR-II intensity profile measured along the green dashed bar with its peak fitted to a Gaussian function.

half-life of DSPE-mPEG coated SWNTs (~5 h),[24] the injected CS-SWNTs acted as vascular contrast agents and revealed the structures of tumor vessels (Figure 4) with down to <10 μm spatial resolution (Figure 4b inset) focused in a plane ~2 mm deep inside the tumor through a 10× objective. This demonstrated the use of ~1200 nm emitting CS-SWNTs to image and resolve tumor blood vessels ~2 mm deep under the skin, using a much lower injected SWNT dose of 0.16 mg/kg of body weight (or 3 μg per mouse) than needed with unsorted SWNTs (2.5 mg/kg of body weight or 50 μg per mouse).[8]

One of the advantages of using chirality separated and resonantly excited SWNTs for biological imaging is the much lower dose needed for injection. Previous study has found excretion of similarly PEGylated but unseparated SWNTs from mice via the biliary and renal pathways without obvious toxicity.[24] Our current work used an injected dose more than an order of magnitude lower than the previous study. All of the healthy mice injected with the chirality separated, low-dose SWNTs have been monitored for up to 4 months and showed no obvious health problems. The use of low-dose, highly homogeneous SWNTs for *in vivo* applications should reduce any possible short- and long-term toxicity, decrease the retention level, and facilitate clearance of SWNTs from the body.

dx.doi.org/10.1021/ja307966u | J. Am. Chem. Soc. 2012, 134, 16971−16974

In summary, we successfully separated and used brightly fluorescent, highly homogeneous SWNT fluorophores consisting of predominantly (12,1) and (11,3) chiralities for real-time *in vivo* NIR-II fluorescence imaging in mice. The CS-SWNTs were separated based on the structure-dependent interaction of SWNTs with an allyl dextran size-exclusion gel. Due to strong resonance with the 808 nm laser and elimination of metallic nanotubes and bundles, the CS-SWNTs showed a ∼5.0-fold higher fluorescence brightness compared to unsorted HiPCO SWNTs. The surfactant exchanged biocompatible (12,1) and (11,3) CS-SWNTs were useful for deep organ imaging and registration as well as high-magnification hindlimb vessel imaging at a dose 6 times lower than needed for unsorted SWNTs, which could help reduce toxicity concerns for nanotubes *in vivo*. This could greatly facilitate the widespread use of SWNT-based NIR-II fluorophores for biomedical applications.

■ ASSOCIATED CONTENT

Ⓢ Supporting Information

Detailed characterization of CS-SWNTs and a video of *in vivo* whole-animal fluorescence imaging using intravenously injected (12,1) and (11,3) CS-SWNTs. This material is available free of charge via the Internet at http://pubs.acs.org.

■ AUTHOR INFORMATION

Corresponding Author

hdai@stanford.edu

Author Contributions

[§]These authors contributed equally.

Notes

The authors declare no competing financial interest.

■ ACKNOWLEDGMENTS

This study was supported by grants from the NIH-NCI (5R01CA135109-02) and MARCO MSD (5710002717-5) to H.D., Stanford Graduate Fellowship to G.H. and National Science Foundation under award no. CHE-1137395 to C.L.C.

■ REFERENCES

(1) Liu, Z.; Tabakman, S.; Welsher, K.; Dai, H. J. *Nano Res.* **2009**, *2*, 85.
(2) Hong, G. S.; Tabakman, S. M.; Welsher, K.; Chen, Z.; Robinson, J. T.; Wang, H. L.; Zhang, B.; Dai, H. J. *Angew. Chem., Int. Ed.* **2011**, *50*, 4644.
(3) Hong, G. S.; Wu, J. Z.; Robinson, J. T.; Wang, H. L.; Zhang, B.; Dai, H. J. *Nat. Commun.* **2012**, 3.
(4) Liu, Z.; Fan, A. C.; Rakhra, K.; Sherlock, S.; Goodwin, A.; Chen, X. Y.; Yang, Q. W.; Felsher, D. W.; Dai, H. J. *Angew. Chem., Int. Ed.* **2009**, *48*, 7668.
(5) Liu, X. W.; Tao, H. Q.; Yang, K.; Zhang, S. A.; Lee, S. T.; Liu, Z. A. *Biomaterials* **2011**, *32*, 144.
(6) Wang, X. J.; Wang, C.; Cheng, L.; Lee, S. T.; Liu, Z. *J. Am. Chem. Soc.* **2012**, *134*, 7414.
(7) Welsher, K.; Sherlock, S. P.; Dai, H. J. *Proc. Natl. Acad. Sci. U.S.A.* **2011**, *108*, 8943.
(8) Welsher, K.; Liu, Z.; Sherlock, S. P.; Robinson, J. T.; Chen, Z.; Daranciang, D.; Dai, H. J. *Nat. Nanotechnol.* **2009**, *4*, 773.
(9) Bachilo, S. M.; Balzano, L.; Herrera, J. E.; Pompeo, F.; Resasco, D. E.; Weisman, R. B. *J. Am. Chem. Soc.* **2003**, *125*, 11186.
(10) Bachilo, S. M.; Strano, M. S.; Kittrell, C.; Hauge, R. H.; Smalley, R. E.; Weisman, R. B. *Science* **2002**, *298*, 2361.
(11) Krupke, R.; Hennrich, F.; von Lohneysen, H.; Kappes, M. M. *Science* **2003**, *301*, 344.
(12) Ghosh, S.; Bachilo, S. M.; Weisman, R. B. *Nat. Nanotechnol.* **2010**, *5*, 443.
(13) Tu, X. M.; Manohar, S.; Jagota, A.; Zheng, M. *Nature* **2009**, *460*, 250.
(14) Liu, H. P.; Nishide, D.; Tanaka, T.; Kataura, H. *Nat. Commun.* **2011**, 2.
(15) Miyata, Y.; Shiozawa, K.; Asada, Y.; Ohno, Y.; Kitaura, R.; Mizutani, T.; Shinohara, H. *Nano Res* **2011**, *4*, 963.
(16) Moshammer, K.; Hennrich, F.; Kappes, M. M. *Nano Res.* **2009**, *2*, 599.
(17) Tanaka, T.; Jin, H.; Miyata, Y.; Fujii, S.; Suga, H.; Naitoh, Y.; Minari, T.; Miyadera, T.; Tsukagoshi, K.; Kataura, H. *Nano Lett.* **2009**, *9*, 1497.
(18) Liu, H.; Feng, Y.; Tanaka, T.; Urabe, Y.; Kataura, H. *J. Phys. Chem. C* **2010**, *114*, 9270.
(19) Crochet, J. J.; Hoseinkhani, S.; Luer, L.; Hertel, T.; Doorn, S. K.; Lanzani, G. *Phys. Rev. Lett.* **2011**, 107.
(20) Murakami, Y.; Maruyama, S. *Phys. Rev. B* **2009**, 79.
(21) Kam, N. W. S.; O'Connell, M.; Wisdom, J. A.; Dai, H. J. *Proc. Natl. Acad. Sci. U.S.A.* **2005**, *102*, 11600.
(22) Matthes, R.; Cain, C. P.; Courant, D.; Freund, D. A.; Grossman, B. A.; Kennedy, P. A.; Lund, D. J.; Mainster, M. A.; Manenkov, A. A.; Marshall, W. J.; McCally, R.; Rockwell, B. A.; Sliney, D. H.; Smith, P. A.; Stuck, B. E.; Tell, S. A.; Wolbarsht, M. L.; Zheltov, G. I.; Cheney, F.; McLin, L.; Ness, J.; Schulmeister, K.; Steinman, R. M.; Sutter, E.; Zwick, H.; Protect, I. C. N.-I. R. *Health Phys.* **2000**, *79*, 431.
(23) Hillman, E. M. C.; Moore, A. *Nat. Photonics* **2007**, *1*, 526.
(24) Liu, Z.; Davis, C.; Cai, W. B.; He, L.; Chen, X. Y.; Dai, H. J. *Proc. Natl. Acad. Sci. U.S.A.* **2008**, *105*, 1410.